Supporting Information

Simulating and explaining passive air sampling rates for semi-volatile compounds on polyurethane foam passive samplers

Nicholas T. Petrich[1,2], Scott N. Spak[1,2,3*], Gregory R. Carmichael[1,2,4], Dingfei Hu[1,5], Andres Martinez[1,5], Keri C. Hornbuckle[1,2,5*]

1. Department of Civil & Environmental Engineering, The University of Iowa, Iowa City, Iowa, United States, 52242
2. Center for Global and Regional Environmental Research, The University of Iowa, Iowa City, Iowa, United States, 52242
3. Public Policy Center and School of Urban & Regional Planning, The University of Iowa, Iowa City, Iowa, United States, 52242
4. Department of Chemical & Biochemical Engineering, The University of Iowa, Iowa City, Iowa, United States, 52242
5. IIHR-Hydroscience and Engineering, The University of Iowa, Iowa City, Iowa, United States, 52242

Contents

WRF Meteorology Simulation

The Weather Research and Forecasting model (WRF) version 3.3[1, 2] simulated hourly meteorology for 2008 over three horizontal domains (Figure 1), each with 35 vertical layers from the surface to the lower stratosphere (1000 Pa).

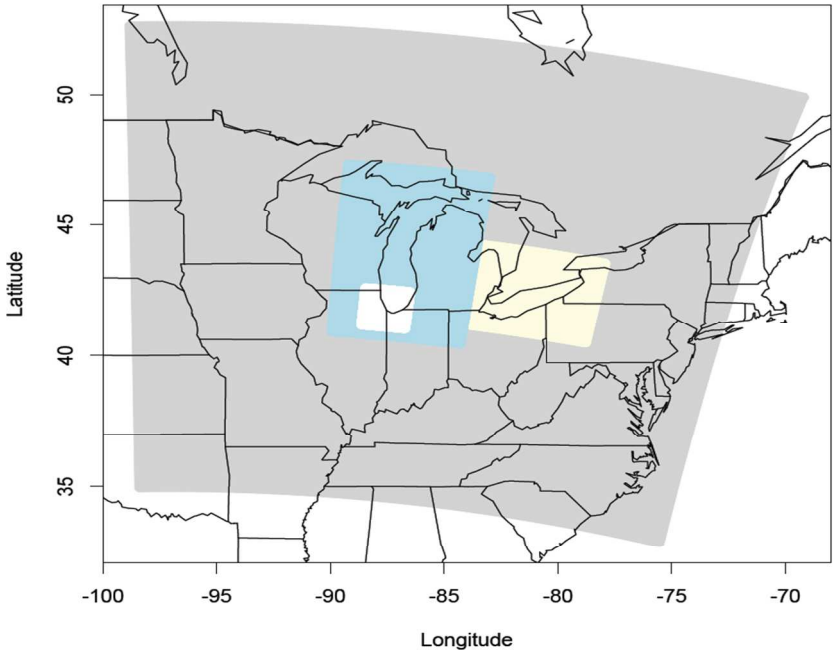

Figure 1. WRF modeling domains: 12 km regional (grey), 4 km airshed over Lake Michigan (light blue) and Lake Erie (maize), and a nested 1.33 km domain over the Chicago metropolitan area (white)

The WRF simulations consisted of 12 x 12 km regional coarse domain located over the upper Midwest and Northeast United States and including all sites in the Integrated Atmospheric Deposition Network (IADN). Nested inside the regional domain is a fine resolution 4 x 4 km domain over Lake Michigan, and then a 1.33 x 1.33 km domain over the urban complex of Chicago. Results are presented for the 1.33 km simulation. The physics parameterizations in WRF simulations are as follows: the Lin scheme, used for real –data high resolution simulations for snow, ice and graupel process was for chosen for microphysics:[3] RRTM scheme longwave

radiation,[4] Goddard scheme for shortwave radiation;[5] MM5 similarity scheme based on Monin-Obukhov scheme for surface layer; Noah land surface model[6] incorporating soil temperature and moisture in four layer fractional snow cover and frozen soil physics; Yonsei University scheme for planetary boundary layer closure;[7] and the Kain-Fritsch scheme for the 12 km domain and the Grell 3D scheme for the 4 km and 1.33 km domains for cumulus convection.[1, 8] Meteorological boundary conditions were based on the North American Regional Reanaylsis (NARR), which included to the use of gridded analysis and observational nudging.[9, 10] Gridded analysis nudging for horizontal wind vectors, temperature, and water vapor mixing ratio from NARR was conducted every three hours above the planetary boundary layer, to reduce large-scale errors in these atmospheric variables.[10]

Meteorological Evaluation

WRF meteorology was evaluated using METSTAT,[11] comparing hourly simulated meteorology with observations from automated weather observing systems (AWOS) stations at the 16 airports in the 1.33 km domain, and calculates descriptive statistics for meteorology of importance for chemical transport: mean biases, root mean square error (RMSE), and correlation coefficient (R^2), for wind speed (WS), wind direction (WD), and temperature (T).[11]

Results (Table 1) indicate WRF met or exceeded community standards during most of the simulation, with performance statistics consistent with established benchmarks for regional meteorological modeling in air quality studies.[12] While annual WS RMSE and T bias were slightly higher than the goals (2.0 m/s and ± 0.5K),[12] the model met all goals for December - June, during the majority of the PUF deployments simulated.

Table 1. Meteorological evaluation for the 1.33 km WRF simulation: hourly mean bias, RMSE, and R^2

	Wind Speed (m/s)			Wind Direction (˚)		Temperature (˚C)		
Month	**Mean Bias**	**RMSE**	**R^2**	**Mean Bias**	**R^2**	**Mean Bias**	**RMSE**	**R^2**
January	-0.08	1.72	0.72	-1.01	0.69	-1.75	3.30	0.90
February	-0.19	1.66	0.79	-2.20	0.55	2.91	0.04	0.91
March	0.08	1.71	0.70	-1.60	0.62	1.56	2.63	0.87
April	0.34	1.88	0.80	0.34	0.45	2.86	3.31	0.89
May	0.20	1.77	0.74	-3.05	0.67	2.71	3.17	0.87
June	0.44	1.94	0.62	1.07	0.46	3.13	3.43	0.83
July	2.03	2.70	0.16	14.22	0.02	-1.37	3.38	0.58
August	1.19	2.35	0.06	21.47	0.00	-3.35	4.84	0.77
September	-0.80	2.32	0.06	46.27	0.01	-4.83	7.39	0.36
October	-2.85	3.37	0.03	-5.53	0.00	9.33	7.03	0.42
November	-3.30	3.87	0.01	-8.32	0.02	-3.76	6.25	0.21
December	-0.25	1.85	0.76	0.20	0.79	-0.18	2.56	0.91
Annual	**-0.27**	**2.26**	**0.45**	**5.16**	**0.36**	**0.61**	**3.94**	**0.71**

Diffusive and Advective Sampling Rates

Here we provide the complete expression or value for each aspect of the sampling rate calculation, Equation 4 in the text. Molecular diffusivity of a gas-phase compound in the atmosphere was calculated using water vapor as a reference compound, from the molecular weights (MW) and molar volumes (V) of air and water, temperature (T), pressure (P), and the molecular weight ratio of the compound and water, as shown in Equation SI-1 [13, 14]:

$$D_{PCB\,a} = \frac{(10^{-3} * T^{1.75} * [(1/MW_{Air}) + (1/MW_{water})]^{-.5})}{(P * (1/101325) * [V_{Air}^{(1/3)} + V_{water}^{(1/3)}]^2)} * \left(\frac{MW_{PCB}}{MW_{water}}\right)^{-(0.5)} \quad (1)$$

Where T is the ambient air temperature (K), MW_{Air} is the molecular weight of air (28.97 gmole^{-1}), MW_{Water} is the molecular weight of water (18.015 g mole^{-1}), P is the atmospheric pressure (atm), V_{Air} is the molecular volume of air (20.1 cm^{3}mole^{-1}), V_{water} is the molecular volume of water (9.5 cm^3 mole^{-1}), and MW_{PCB} is the molecular weight of the PCB congener being analyzed (g mole^{-1}).

The advective contribution to Kv considers gas-phase compounds within moist air as the product of v, V_A, and L, where L is diameter of the PUF disk (0.14 m). To compute kinematic

viscosity (ν) the dynamic viscosity of moist air (η_m) and air density (ρ) are calculated as a function of the viscosity of air and water and the molar fractions of air and water, as indicated in Equation SI-2:

$$\eta_m = (X_a * \eta_a + X_w * \eta_w) * (1 + \frac{X_w - X_w^2}{a}) \quad (2)$$

in which X_a is the molar fraction of air in an atmospheric parcel, η_a is the viscosity of air (kg m^{-1}-s^{-1}), X_w is the molar fraction of water in a an air parcel, η_w is the viscosity of water (kg m^{-1}-s^{-1}), and a is an empirical factor dependent on temperature.[15] Air and water viscosity are calculated as:

$$\eta_a = \frac{17.78*(4.58T_r - 1.67)^{5/8} * 10^{-7}}{\zeta_a} \quad (3)$$

$$\eta_w = \frac{(7.55T_r - 0.55)Z_c^{-5/4} * 10^{-7}}{\zeta_w} \quad (4)$$

where T_r is the ratio of the critical temperature for air (132.206) to absolute temperature and is dimensionless, ζ_a is the pseudocritical constant for air (0.038474) (dimensionless), ζ_w is the pseudocritical constant for water (0.0192) (dimensionless), and Z_c is critical compressibility factor for water (0.231) (dimensionless) [16]. Equation SI-3 and Equation SI-4 are used alongside the molar fractions of air and water in an air parcel to compute η_m:

$$X_a = \frac{\frac{1}{Q_V} * \frac{1}{MW_a}}{(Q_v \frac{1}{MW_w} * \frac{P}{R_d T}) + \frac{1}{Q_V} * \frac{1}{MW_a}} \quad (5)$$

$$X_w = \frac{(Q_v \frac{1}{MW_w} * \frac{P}{R_d T})}{(Q_v \frac{1}{MW_w} * \frac{P}{R_d T}) + \frac{1}{Q_V} * \frac{1}{MW_a}} \quad (6)$$

in which Q_v is the water vapor mixing ratio (kg kg^{-1}) and R_d is the specific gas constant of dry air (287.05 J Kg^{-1}-K^{-1}).Moist air density was used instead of dry air density, since the atmosphere is approximately 4% water vapor and the molecular weight of water is less than the molecular weight or air:

$$\rho_m = \frac{P_d}{R_d * T} + \frac{P_v}{R_v * T} \quad (7)$$

where P_d is the partial pressure of dry air (Pa) which is the product of X_a and P, P_v is the partial pressure of water vapor (Pa) determined as the product of X_v and P, and R_v is the specific gas constant for water vapor (461.495 J Kg^{-1}-K^{-1}) [17]. The kinematic viscosity (*v,* m s^{-2}) is the ratio of measured internal resistance (η_m) around the PUF disk and ρ_m, indicated in Equation SI-8:

$$\nu = \frac{\eta_m}{\rho_m} \qquad (8)$$

We considered α and β values consistent with flow over a flat plate, where α=0.5 for laminar flow and α=0.9 for turbulent flow (internal air velocities ≥ 0.5 m s^{-1}). In both cases, β= 0.33.

Advective Mass Transfer Coefficient (γ)

The γ term is the only empirical parameter in the model, and is determined by calibration of the model with results of the depuration experiments. We expected a single static parameter across all depuration experiments, but found that γ exhibits some dependence on wind speed and temperature, indicating that our model does not completely capture the effect of meteorology. However, this dependence is small. We quantified these effects through multiple linear regression (MLR) (equations 9 and 10). In Table 2, we report the values of gamma without this correction and with correction, as "Sample Specific g" and "MLR g", respectively. Figure 2 shows that V_A explains 76% of variability in γ for each PUF's PCB 28 sampling rate, while T explains 46%. Multiple linear regression on V_A and T for the seven observations yielded

$\gamma_{PCB28} = -0.75 + 0.78 * V_A + 0.0034 * T - 0.0031 * V_A * T$ (9)

for the advective approach of Tuduri et al. (2006), and

$\gamma_{PCB28} = -0.28 + 0.077 * V_A + 0.0013 * T - 0.00031 * V_A * T$ (10)

for the sampling rate dependence on wind angle from May et al. (2011).

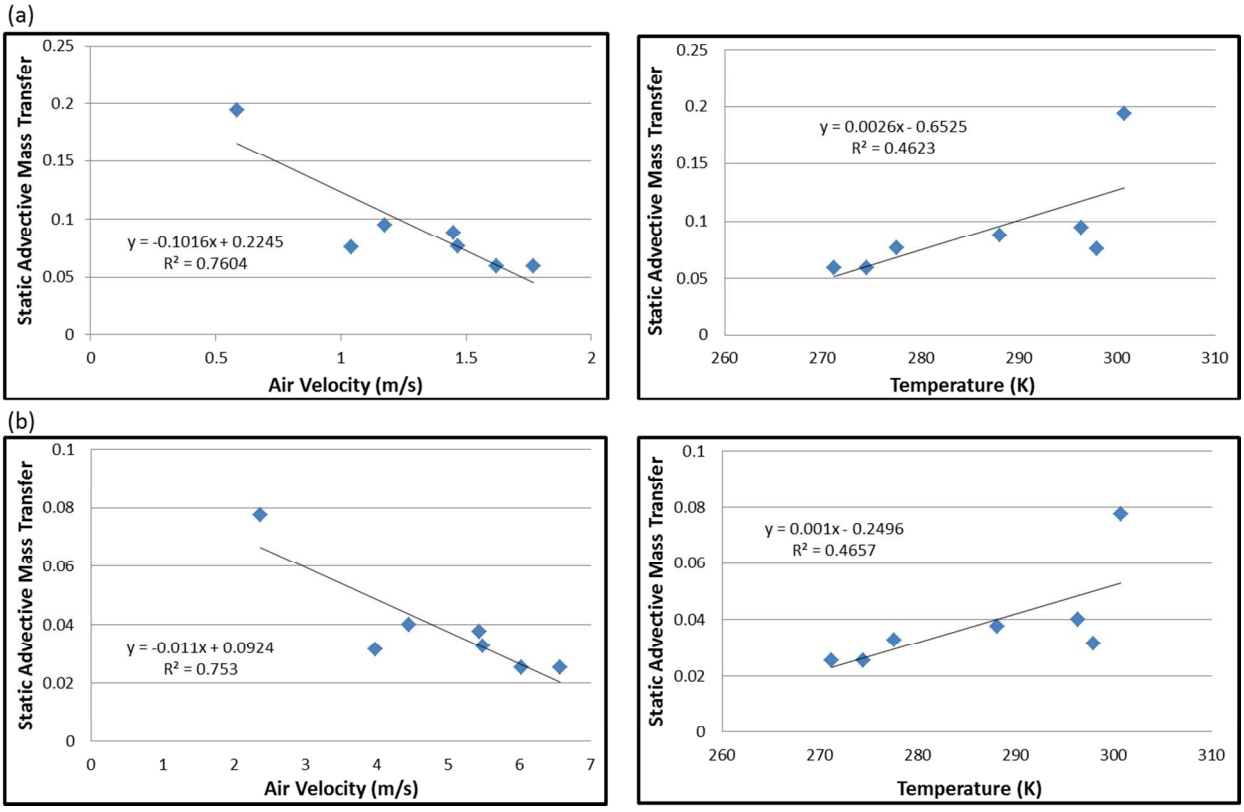

Figure 2. Correlation between γ for PCB 28 with VA (left) and T (right) for two advective approaches: (a) internal air velocity from Tuduri et al. (2006) (b) sampling rate dependence on wind angle as in May et al. (2011).

Table 2 shows that simulated R_s using the empirical R_S dependence on wind angle are nearly identical to those using R_s dependence on internal air velocity within the PAS, differing on average by 2% for median γ and 0.02% for MLR γ. Values for γ are ~50% smaller, as advection is calculated using the higher external wind speed.

Table 2. Modeled and depuration PCB 28 R_S for each depuration compound sample, including R_S dependence on vertical wind angle. R_S and γ reported for sample-specific fit, multiple linear regression, and median values. A median value for γ of 0.033 is found from all sites.

					Average Model R_S (m^3/d)	
Site	Sampling Period	Sample Specific γ	MLR γ	Depuration R_S (m^3/d)	Median γ	MLR γ
Dewey	1/17 – 2/26	0.03	0.03	5.00	6.49	5.98
Dawes	2/22 – 4/11	0.03	0.03	5.53	5.58	5.32
Corkery	4/18 – 5/16	0.04	0.03	5.94	5.21	4.39
Gresham	5/16 – 7/31	0.03	0.05	3.84	4.02	5.58
Chase	6/30 – 8/11	0.08	0.07	6.79	2.89	6.28
St. Elizabeth	8/11 – 9/19	0.04	0.04	5.67	4.67	5.50
Webster	11/13 – 12/19	0.03	0.02	5.06	6.55	4.84
	Average	**0.04**	**0.04**	**5.40**	**5.06**	**5.41**

PCB 111 Sampling Rate Evaluation

Table shows the importance of γ adjustment from multiple linear regression on V_A and T observed in each deployment for PCB 111 when using γ values scaled by log(K_{OA}) from PCB 28, where

$$\gamma_{SVOC} = \gamma_{28} * \frac{Log\ K_{OA}\ (SVOC)}{Log\ K_{OA}\ (PCB\ 28)} \qquad (11)$$

After scaling, difference with PCB 111 depuration compound R_S is slightly higher for each deployment than for PCB 28, and MLR adjustment for γ_{28} more important to reducing that difference.

Table 3. Median γ and site specific multiple linear regression (MLR) γ for PCB 111, and average modeled and observed R, including normalized mean error and bias for each sampling site using hourly de-biased WRF meteorology. A median value for γ of 0.086 is found from all sites.

				Average Model R_S (m^3/d)	
Site	**Sampling Period**	**Scaled MLR γ**	**Depuration R_S (m^3/d)**	**Median γ**	**Scaled γ**
Dewey	1/17 – 2/26	0.08	4.30	6.95	6.55
Dawes	2/22 – 4/11	0.08	5.84	5.95	5.74
Corkery	4/18 – 5/16	0.07	6.52	5.55	4.62
Gresham	5/16 – 7/31	0.13	7.90	4.18	6.09
Chase	6/30 – 8/11	0.21	7.85	2.88	6.80
St. Elizabeth	8/11 – 9/19	0.11	5.97	4.92	5.97
Webster	11/13 – 12/19	0.06	4.74	7.03	5.20
	Average	**0.11**	**6.16**	**5.35**	**5.85**

Process Uncertainty in Sampling Rate

Sensitivity analysis at the Dawes School sampling site from 2/22/2008 – 4/11/2008 PUF deployment analyzed the individual impacts of each simulated process on total R_S: advection, meteorology source, and temperature. The net range in average sampling rate was 0.48 m^3 d^{-1} (9.5%), and the average hourly difference in sampling rate between the upper bound and lower bound of the Dawes time series was 1.15 ± 0.56 m^3 d^{-1} (22%) with minimum and maximum differences of 0.28 and 3.70 m^3 d^{-1}, respectively.

The smallest variabillity in R_S was seen with simulated meteorology and ambient air temperature. For each advective approach, de-biased meteorology and internal chamber temperature (T_{PAS}) estimation led to the largest range in total R_S, as well as the highest average

R_S. Sensitivity to meteorology data source is minimal; hourly debiased simulated meteorology increases average R_S and variability slightly, by 1.8 %. The use of ambient vs. surface temperature plays an important role in R_S (7.3%) over the deployment period. Although T_{PAS} was approximated as WRF T_{skin}, we anticipate larger differences in R_S using observed T_{PAS}, as temperatures in the metal chamber would be warmer than surface temperature during the day and cooler at night.

References

1. User's Guide for the Advanced Research WRF (ARW) Modeling System Version 3.3 http://www.mmm.ucar.edu/wrf/users/docs/user_guide_V3.3/contents.html
2. Skamarock, W. C.; Klemp, J. B.; Dudhia, J.; Gill, D. O.; Barker, D. M.; Duda, M. G.; Huang, X.-Y.; Wang, W.; Power, J. G., A Description of the Advanced Research WRF Version 3. In National Center for Atmospheric Research: Boulder, Colarado, 2008; Vol. NCAR/TN-475+STR, p 125.
3. Lin, Y. L.; Farley, R. D.; Orville, H. D., Bulk Parameterization of the Snow Field in a Cloud Model. *Journal of Climate and Applied Meteorology* **1983,** *22*, (6), 1065-1092.
4. Mlawer, E. J.; Taubman, S. J.; Brown, P. D.; Iacono, M. J.; Clough, S. A., Radiative transfer for inhomogeneous atmospheres: RRTM, a validated correlated-k model for the longwave. *J. Geophys. Res.-Atmos.* **1997,** *102*, (D14), 16663-16682.
5. Chou, M. D.; Suarez, M. J., A shorthwave radiation parameterication for atmospheric studies. *NASA* **1999,** *TM-104606*.
6. LeMone, M. A.; Tewari, M.; Chen, F.; Alfieri, J. G.; Niyogi, D., Evaluation of the Noah Land Surface Model Using Data from a Fair-Weather IHOP_2002 Day with Heterogeneous Surface Fluxes. *Mon. Weather Rev.* **2008,** *136*, (12), 4915-4941.
7. Hu, X. M.; Nielsen-Gammon, J. W.; Zhang, F. Q., Evaluation of Three Planetary Boundary Layer Schemes in the WRF Model. *J. Appl. Meteorol. Climatol.* **2010,** *49*, (9), 1831-1844.
8. G.A.;, G.; Dudhia, J.; Stauffer, D. R. *A Secription of the Fifth-Generation Penn State.NCAR Mecoscale Modell (MM5)*; National Center for Atmospheric Research NAtional Oceanic and Atmospehric Administration Pennsylvania State University: Boilder, CO, 1994; p 128.
9. Mesinger, F.; DiMego, G.; Kalnay, E.; Shafran, P.; Ebisuzaki, W.; Dusan, J.; Woollen, J.; Mitchell, K.; Rogers, E.; Ek, M.; Fan, Y.; Grumbine, R.; Higgins, W.; Hong, L.; Lin, Y.; Manikin, G.; Parrish, D.; Shi, W., North American Regional Reanalysis. In American Meteorological Society: 2004; p 34.
10. Baker, D. D., T.; Ku, M.; Hao, W.; Sistia, G.; Kiss, M.; Johnson, M.; Brown, D.;, Sensitivity Testing of WRF Physics Parameterizations for Meterological Modeling and Protocol in Support of Regional SIP Air Quality Modeling in the OTR. Ozonte Transport ., Ed. 2010; p 73.
11. *METSTAT*, Environ International Corporation: 2009.
12. Emery, C.; Tai, E.; Yarwwood, G., Enhanced Meteorological Modeling and Performance Evaluation for the Two Texas Ozone Episodes. In Commision, T. N. R. C., Ed. Environ International Corporation: Novato, CA, 2001.